

Simultaneous Wireless Power Transfer and Modulation Classification

Rahul Gupta and Ioannis Krikidis

Department of Electrical and Computer Engineering, University of Cyprus

Email: {gupta.rahul, krikidis.ioannis}@ucy.ac.cy

Abstract—This work proposes a new simultaneous wireless power transfer and modulation classification (SWPTMC) scheme appropriate for internet of things (IoT) applications. The problem of SWPTMC is investigated for various modulation formats, i.e., quadrature phase-shift-keying (QPSK), $\pi/4$ -QPSK, offset QPSK (OQPSK), 16-pulse amplitude modulation (16-PAM), 16-quadrature amplitude modulation (16-QAM), and minimum shift keying (MSK). We propose three receiver architectures, i.e., an integrated receiver, a separate receiver with power splitting (PS), and a separate receiver with energy harvesting (EH)-based classification; all the architectures are studied under a non-linear model with a certain sensitivity and saturation level. Also, we derive the average harvested power over a Rayleigh fading channel for the different modulation formats. Two different approaches are used for the blind modulation classification (MC) algorithm: one for the intermediate frequency signal and the other for the baseband signal. Both the MC algorithms are based on the higher-order cumulants and cyclic cumulants of the received signal. The cyclic cumulants use the non-zero cycle frequency position, while the cumulants use threshold values for classifying modulation formats. Monte Carlo simulations are used to evaluate the performance of the proposed SWPTMC schemes. The results show that we can simultaneously harvest power without much affecting the classifier performance. Moreover, with an integrated receiver, we can simultaneously perform MC and harvest power without the requirement of PS circuit.

Index Terms—Cumulants, cyclic cumulants, energy harvesting, modulation classification, wireless power transfer.

I. INTRODUCTION

ENERGY-efficient transmission is one of the primary concerns in modern wireless networks, such as wireless sensor networks and Internet of Things (IoT) due to the limited lifespan of fixed energy supplies. At the same time, high costs and practical difficulty of replacing frequent batteries motivate remote energy recharging technologies. Wireless power transfer (WPT) through radio-frequency (RF) signals has recently emerged as a candidate technology for providing power to remotely located sensors and IoT devices [1], [2]. The WPT concept is extended to the simultaneous wireless information and power transfer (SWIPT), which allows data and power to be transmitted through the same electromagnetic waveform.

This work was supported by the European Regional Development Fund and the Republic of Cyprus through the Research and Innovation Foundation, under the projects INFRASTRUCTURES/1216/0017 (IRIDA) and EXCELLENCE/1216/0376 (SWITCH). It has also received funding from the European Research Council (ERC) under the European Union's Horizon 2020 research and innovation programme (Grant agreement No. 819819).

SWIPT has recently gained significant attention as an integrated approach for information decoding (ID) and energy harvesting (EH) [3]–[5]. Practical SWIPT receivers for ID and EH have been proposed by using time-switching (TS) and power splitting (PS) schemes using linear and non-linear energy harvesting models [6]–[9]. In the PS scheme, the incoming RF signal is divided into two components by the power splitter and the split signals are fed into the ID and EH circuit, respectively. On the other hand, the TS scheme antenna switches periodically between ID and EH circuits. It also requires precise scheduling of information/energy and time synchronization. In fact, it is recognized that the PS scheme achieves better ID and EH trade-off performance than the TS scheme [8], [9]. In addition, the high peak-to-average power ratio (PAPR) modulation scheme results in improved EH performance for the PS scheme [7].

Classification of modulation formats is a very important process of smart receivers to ensure correct demodulation. It plays a significant role in the military, signal intelligence, and civilian applications. Blind estimation is bandwidth efficient as it does not require pilot symbols or training sequences in the estimation process [10]. The blind modulation classification (MC) algorithms can be divided into two general categories: likelihood-based (LB) and feature-based (FB) algorithms. The LB algorithms require signal preprocessing tasks and suffer from higher computational complexity [10]. Whereas FB algorithms are easy to implement and computational complexity is much lower than LB algorithms [11]–[16]. The higher-order cumulants and moments-based MC algorithms employ threshold values to classify the modulation formats [11]–[13]. The cyclic cumulants-based methods discussed in [14]–[16] are more robust and use the non-zero cycle frequency position to identify the modulation schemes.

Within this context, the prospect of integrating intelligent transceiver systems with WPT creates a need for technology that can transfer both power and modulation information simultaneously to the end-devices and plays a significant role in military, intelligence, IoTs, and as well as control and adaptation systems. In this paper, we propose a new receiver architecture that simultaneously harvests power and performs blind MC; this joint design introduces a new concept which is called simultaneous wireless power transfer and modulation classification (SWPTMC). We propose three receiver architectures under a non-linear harvesting model with a certain

sensitivity and saturation level: (a) an integrated receiver that simultaneously harvests energy and performs blind MC at the intermediate frequency (IF) level without the need of PS circuit; (b) a separate receiver, which uses the MC circuit at the baseband level, therefore a PS scheme is required for further processing of the received signal; (c) a separate receiver with EH-based classifier uses the harvested power as additional information to further improve the classification accuracy of MC circuit. The proposed MC algorithm can be applied to a wide range of modulations, i.e., quadrature phase-shift-keying (QPSK), 16-pulse amplitude modulation (16-PAM), $\pi/4$ -QPSK, minimum shift keying (MSK), offset QPSK (OQPSK), and 16-quadrature amplitude modulation (16-QAM). It is based on the combination of higher-order cumulants and cyclic cumulants. The cyclic cumulants use the non-zero cycle frequency position, while the higher-order cumulants use threshold values for classifying modulation formats. To the best of the authors' knowledge, this is the first work in the literature focused on SWPTMC scheme.

II. SIGNAL MODEL

We consider a SWPTMC system consisting of a transmitter and receiver as shown in Fig. 1. The transmitter sends the modulated data signal with an average transmission power of \mathcal{P}_{tx} in each time slot. The receiver divides the received signal into two components, i.e., for the blind MC with PS ratio $1-\rho$ and the other one is for EH with power ratio ρ , where ρ is the PS factor. Both the transmitter and the receiver have a single antenna. The transmitted continuous-time domain passband signal is given as

$$\begin{aligned} x(t) &= \Re \left\{ s(t) e^{j(2\pi f_c t + \phi)} \right\}, \\ &= s_I(t) \cos(2\pi f_c t + \phi) + s_Q(t) \sin(2\pi f_c t + \phi), \end{aligned} \quad (1)$$

where ϕ is the carrier phase and f_c is the IF carrier frequency. The in-phase (I) and quadrature (Q) components of the transmitted signal $s(t)$ are given as: $s_I(t) = \sum_{k=0}^{K-1} a_I(k)g(t-kT)$ and $s_Q(t) = \sum_{k=0}^{K-1} a_Q(k)g(t-kT)$, respectively, where $a(k) = a_I(k) + ja_Q(k)$, K is the number of symbols, $g(t)$ is the root raised cosine (RRC) pulse shape filter, and T is the symbol period. For QPSK, OQPSK, MSK: $a_I(k), a_Q(k) \in \{\pm 1/\sqrt{2}\}$; $\pi/4$ -QPSK: $a_I(k), a_Q(k) \in \{\pm 1, \pm 1/\sqrt{2}\}$; 16-PAM: $a_I(k) \in \{\pm(2d-1)/\sqrt{85}\}$, $a_Q(k) = 0$, with $d \in \{1, \dots, 8\}$; and 16-QAM: $a_I(k), a_Q(k) \in \{\pm 3/\sqrt{10}, \pm 1/\sqrt{10}\}$. The continuous-time domain signal at the receiver is modelled as

$$y(t) = \Re \left\{ \sum_{l=0}^{L-1} h(l)x(t-l) + v(t) \right\}, \quad (2)$$

where $v(t)$ is the passband additive white Gaussian noise (AWGN) with zero mean and variance of σ_v^2 and $h(l) = h(0), \dots, h(L-1)$ is the Rayleigh fading coefficients of a multipath channel with L taps having zero mean and variance one. The above received signal is oversampled at rate P/T to get the discrete-time signal as $y[n] = \Re \left\{ \sum_{l=0}^{L-1} h[l]x[n-l] + v[n] \right\}$. The oversampling factor is

defined as $P = F_s/f_s$, where $F_s = 1/T_s$ is the sampling rate, $f_s = 1/T$ is the symbol rate, T_s is the sampling period, and T is the symbol period. At the receiver, we consider a non-linear EH model and the power received at the EH circuit is \mathcal{P}_r . The amount of harvested power can be expressed as [6], [7]

$$\mathcal{P}_{\text{Eh}} = \begin{cases} 0, & \mathcal{P}_r < \mathcal{P}_1; \\ \eta(\mathcal{P}_r - \mathcal{P}_1), & \mathcal{P}_1 \leq \mathcal{P}_r \leq \mathcal{P}_2; \\ \eta\mathcal{P}_2, & \mathcal{P}_r > \mathcal{P}_2, \end{cases} \quad (3)$$

where $\eta \in [0, 1]$ is the RF-EH conversion efficiency, \mathcal{P}_1 is the minimum RF-EH sensitivity level, and \mathcal{P}_2 is the maximum harvested power when the EH circuit meets saturation.

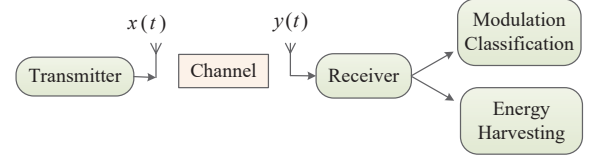


Fig. 1. A basic SWPTMC system model.

III. PRELIMINARIES

A. Higher-order Cumulant

Higher-order cumulants are statistical features of random variables represented by higher-order moments. In this section, we provide the basic definitions of cumulants and moments with their respective sample average estimates. For random processes $y_1[n], \dots, y_p[n]$, the p th-order joint moment and cumulant are defined as [17]

$$M_{y_1, \dots, y_p} = \mathbb{E} \left[\prod_{b=1}^p y_b[n] \right], \quad (4)$$

$$c_{y_1, \dots, y_p} = \sum_d (-1)^{d-1} (d-1)! \prod_{\varrho \in d} \left(\mathbb{E} \left[\prod_{b \in \varrho} y_b[n] \right] \right), \quad (5)$$

where $d = \{1, 2, \dots, p\}$ is the list of all possible partitions and ϱ is the list of all blocks within partition d . When $y_b[n] = y[n]$, $b = 1, \dots, p$, this gives the p th-order moment of the random process $y[n]$ as $M_{[y,p]} = \mathbb{E} [y[n]^p]$. For complex-valued random processes, the mixed moments of order p with q conjugations is given as $M_{[y,p,q]} = \mathbb{E} [y[n]^{p-q} y^*[n]^q]$. Similarly, we obtained the p th-order cumulants and mixed cumulants with q conjugations. The sample average estimates of high-order cumulants can be expressed as

$$\hat{c}_{[y,2,0]} = \frac{1}{N} \sum_{n=1}^N y[n]^2; \quad \hat{c}_{[y,2,1]} = \frac{1}{N} \sum_{n=1}^N |y[n]|^2, \quad (6)$$

$$\hat{c}_{[y,4,0]} = \frac{1}{N} \sum_{n=1}^N y[n]^4 - 3\hat{c}_{[y,2,0]}^2,$$

$$\hat{c}_{[y,4,1]} = \frac{1}{N} \sum_{n=1}^N y[n]^3 y[n]^* - 3\hat{c}_{[y,2,0]} \hat{c}_{[y,2,1]},$$

$$\hat{c}_{[y,4,2]} = \frac{1}{N} \sum_{n=1}^N |y[n]|^4 - |\hat{c}_{[y,2,0]}|^2 - 2\hat{c}_{[y,2,1]}^2, \quad (7)$$

$$\begin{aligned} \hat{c}_{[y,6,3]} &= \frac{1}{N} \sum_{n=0}^{N-1} |y[n]|^6 - 9\hat{c}_{[y,4,2]}\hat{c}_{[y,2,1]} + 18\hat{c}_{[y,2,0]}^3 \\ &\quad - 6\hat{c}_{[y,4,1]}\hat{c}_{[y,2,0]} - 9\hat{c}_{[y,2,1]}|\hat{c}_{[y,2,0]}|^2 \\ &\quad - 18\hat{c}_{[y,2,1]}\hat{c}_{[y,2,0]}^2 - 6\hat{c}_{[y,2,1]}^3 \end{aligned} \quad (8)$$

$$\begin{aligned} \hat{c}_{[y,8,4]} &= \frac{1}{N} \sum_{n=0}^{N-1} |y[n]|^8 - 16\hat{c}_{[y,6,3]}\hat{c}_{[y,2,1]} - |\hat{c}_{[y,4,0]}|^2 \\ &\quad - 18\hat{c}_{[y,4,2]}^2 - 72\hat{c}_{[y,4,2]}\hat{c}_{[y,2,1]}^2 - 24\hat{c}_{[y,2,1]}^4, \end{aligned} \quad (9)$$

where N is the received signal length.

B. Cyclic Cumulant

The Fourier series coefficient of the p th-order time-varying correlation function, $\tilde{c}_{[y,p,q]}[n; \tau]$, is known as cyclic cumulant. The fourth-order cyclic cumulant with zero conjugations at $\tau = 0$ lag is obtained as [14], [15]

$$C_{[y,4,0]}[\alpha; 0] \triangleq \sigma_x^4 \sum_{l=0}^{L-1} h^4[l] e^{4j\phi} \delta[\alpha - 4f_c] + \sigma_v^4 \delta[\alpha], \quad (10)$$

where α is the cycle frequency, $\sigma_x^4 = \text{E}\{x^4[n]\}$, and $\sigma_v^4 = \text{E}\{v^4[n]\}$. In practice, (10) can be estimated as the discrete Fourier transform (DFT) of $y^4[n]$ and can be expressed as

$$\hat{C}_{[y,4,0]}[\alpha; 0] = \frac{1}{N} \sum_{n=0}^{N-1} y^4[n] e^{-j2\pi n\alpha}. \quad (11)$$

Once $\hat{C}_{[y,4,0]}[\alpha; 0]$ is determined, frequency estimation is given by

$$\hat{f} = \arg \max \left| \hat{C}_{[y,4,0]}[\alpha; 0] \right|. \quad (12)$$

IV. PROPOSED RECEIVER ARCHITECTURES

A. Integrated Receiver Architecture with Modulation Classification and Energy Harvesting

A SWPTMC integrated receiver consists of two parts as shown in Fig. 2, i.e., blind MC and EH. The MC is performed at the IF level, hence there is no need of PS circuit. In addition, there is no compromise of the signal-to-noise ratio (SNR) at the receiver, resulting in a significant improvement in spectral efficiency and coverage.

1) *Modulation Classification*: The proposed modulation classifier can be applied to a larger pool of modulations, i.e., QPSK, $\pi/4$ -QPSK, OQPSK, 16-PAM, 16-QAM, and MSK over fading channels. It performs in two stages: (a) at the first-stage, we use the fourth-order cyclic cumulants to classify OQPSK, MSK, and $\pi/4$ -QPSK modulation formats; (b) at the second-stage, eight-order cumulant is used to recognize the remaining modulation schemes. The fourth-order cyclic cumulant features at IF level for the various modulation schemes are discussed below.

By using (12), the non-zero cycle frequency for $\pi/4$ -QPSK, MSK, and OQPSK is obtained at $4f_c \pm f_s/2$, $4f_c \pm 2f_s$, and $4f_c$, respectively [14]. For QPSK, 16-QAM, and 16-PAM modulation formats, we get the same feature value i.e., non-zero cycle frequency at $4f_c$ and $4f_c \pm f_s$. Hence,

TABLE I
THEORETICAL VALUE OF EIGHT-ORDER CUMULANT $\hat{c}_{[y,8,4]}$

16-PAM	QPSK	16-QAM
-142.00	-34.00	-13.98

to identify the remaining modulation formats, we use eight-order cumulant with four conjugations. By using (9), we can easily differentiate 16-PAM, QPSK, and 16-QAM modulation formats as shown in Table I and the thresholds can easily be obtained by using the likelihood ratio test [10], [11].

2) *Energy Harvesting*: The received signal at the EH circuit is $y_{\text{er}}(t) = y(t) + w_c(t)$, where $w_c(t)$ is the rectenna circuit AWGN noise with zero mean and variance of σ_c^2 . From the received signal $y_{\text{er}}(t)$, we can find the power for the i -th constellation point as $\mathcal{P}_{r_i} \approx a\mathcal{P}_{x_i}$, where $a = |h|^2$ is the fading power gain. Since, we consider normalized Rayleigh fading, the probability density function of a is given by $f_{\mathcal{A}}(a) = e^{-a}$ and \mathcal{P}_{x_i} is the transmit power for the i -th constellation point. By using (3), the amount of harvested power $\mathcal{P}_{\text{Eh}_i}$ under fading power gain a during one symbol period is obtained as

$$\mathcal{P}_{\text{Eh}_i} = \begin{cases} 0, & \mathcal{P}_{r_i} < \mathcal{P}_1; \\ \eta(a\mathcal{P}_{x_i} - \mathcal{P}_1), & \mathcal{P}_1 \leq \mathcal{P}_{r_i} \leq \mathcal{P}_2; \\ \eta\mathcal{P}_2, & \mathcal{P}_{r_i} > \mathcal{P}_2, \end{cases} \quad (13)$$

From the above equation, we can calculate the average harvested power $\bar{\mathcal{P}}_{\text{Eh}}$ as

$$\begin{aligned} \bar{\mathcal{P}}_{\text{Eh}} &= \sum_{i=1}^M p_i \int_0^{\infty} \mathcal{P}_{\text{Eh}_i} f_{\mathcal{A}}(a) da, \\ &= \frac{\eta}{M} \sum_{i=1}^M \left(\int_{\frac{\mathcal{P}_1}{\mathcal{P}_{x_i}}}^{\frac{\mathcal{P}_2}{\mathcal{P}_{x_i}}} (a\mathcal{P}_{x_i} - \mathcal{P}_1) e^{-a} da + \int_{\frac{\mathcal{P}_2}{\mathcal{P}_{x_i}}}^{\infty} \mathcal{P}_2 e^{-a} da \right), \\ &= \frac{\eta}{M} \sum_{i=1}^M \left(\mathcal{P}_{x_i} \left(e^{-\frac{\mathcal{P}_1}{\mathcal{P}_{x_i}}} - e^{-\frac{\mathcal{P}_2}{\mathcal{P}_{x_i}}} \right) + \mathcal{P}_1 e^{-\frac{\mathcal{P}_2}{\mathcal{P}_{x_i}}} \right), \end{aligned} \quad (14)$$

where $p_i = 1/M$ is the symbol transmit probability. From [18], we get the transmit power \mathcal{P}_{x_i} for different modulation formats. After further simplification, we can obtain the average harvested power as

$$\bar{\mathcal{P}}_{\text{Eh}} = \begin{cases} \eta\mathcal{P}_{\text{tx}} \left(e^{-\frac{\mathcal{P}_1}{\mathcal{P}_{\text{tx}}}} - e^{-\frac{\mathcal{P}_2}{\mathcal{P}_{\text{tx}}}} \right) + \eta\mathcal{P}_1 e^{-\frac{\mathcal{P}_2}{\mathcal{P}_{\text{tx}}}} & \text{for M-PSK,} \\ \frac{3\eta}{2M(M-1)} \sum_{i=1}^M \mathcal{P}_{\text{tx}} Q_i \left(e^{-\frac{2\mathcal{P}_1(M-1)}{3\mathcal{P}_{\text{tx}}Q_i}} - e^{-\frac{2\mathcal{P}_2(M-1)}{3\mathcal{P}_{\text{tx}}Q_i}} \right) \\ \quad + \frac{\eta}{M} \sum_{i=1}^M \mathcal{P}_1 e^{-\frac{2\mathcal{P}_2(M-1)}{3\mathcal{P}_{\text{tx}}Q_i}} & \text{for M-QAM,} \\ \frac{3\eta}{M(M^2-1)} \sum_{i=1}^M \mathcal{P}_{\text{tx}} S_i \left(e^{-\frac{\mathcal{P}_1(M^2-1)}{3\mathcal{P}_{\text{tx}}S_i}} - e^{-\frac{\mathcal{P}_2(M^2-1)}{3\mathcal{P}_{\text{tx}}S_i}} \right) \\ \quad + \frac{\eta}{M} \sum_{i=1}^M \mathcal{P}_1 e^{-\frac{\mathcal{P}_2(M^2-1)}{3\mathcal{P}_{\text{tx}}S_i}} & \text{for M-PAM,} \end{cases} \quad (15)$$

where \mathcal{P}_{tx} is the average transmission power, $Q_i = (2b_i - 1)^2 + (2d_i - 1)^2$, $S_i = (2 \lceil 0.5 |2i - M - 1| \rceil)^2$, $b_i = \lceil |i/\sqrt{M}| \rceil -$

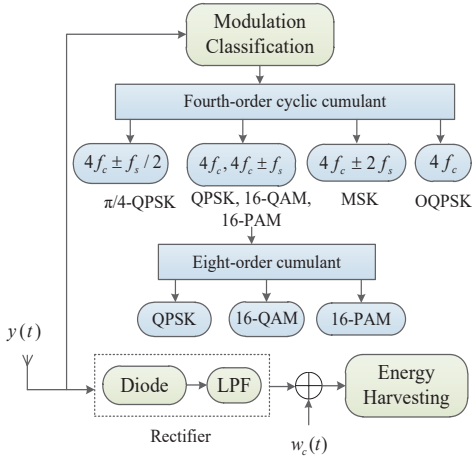


Fig. 2. Block diagram of the proposed integrated receiver architecture.

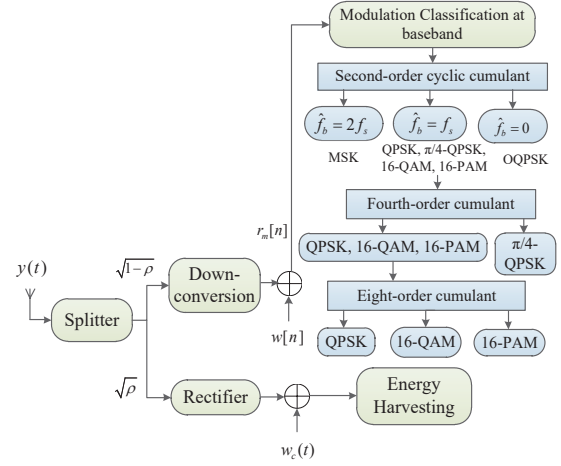


Fig. 3. Block diagram of the proposed separate receiver architecture.

$\sqrt{M} + 1/2]$, and $d_i = \lceil (i \bmod \sqrt{M}) - \sqrt{M} + 1/2 \rceil$, $\lceil \cdot \rceil$ is the ceiling operator, and \bmod is the modulo operator.

B. Receiver Architecture with Separate Modulation Classification and Energy Harvesting

The block diagram of SWPTMC separate receiver is shown in Fig. 3, i.e., it consists of EH and MC circuits. The blind MC is performed at the baseband level, therefore PS scheme is needed for further processing of the received signal. It employs PS scheme to split the received signal into two streams as shown in Fig. 3. One stream for the blind MC with PS ratio $1 - \rho$ and the other stream is for EH with PS ratio ρ , described in detail below.

1) *Modulation Classification*: The received signal at MC circuit is $y_m[n] = \sqrt{1 - \rho} y[n]$. After down conversion, we can obtain the lowpass discrete signal as

$$r_m[n] = \sqrt{1 - \rho} \sum_{l=0}^{L-1} h[l] s[n-l] + w[n], \quad (16)$$

where $w[n]$ is the lowpass AWGN with zero mean and variance of σ_w^2 . The classification performs in three stages: (a) at the first-stage, we use the second-order cyclic cumulants to identify OQPSK and MSK modulation formats; (b) at the second-stage, $\pi/4$ -QPSK modulation is identified using the fourth-order cumulant; (c) at the last-stage, we employ eight-order cumulant to identify the remaining modulation formats. Similar to (11), the second-order cyclic cumulant with one conjugation of the lowpass received signal $r_m[n]$ can be estimated as the DFT of $|r_m[n]|^2$ and can be obtained as

$$\hat{C}_{[r_m, 2, 1]}[\alpha; 0] = \frac{1}{N} \sum_{n=0}^{N-1} |r_m[n]|^2 e^{-j2\pi n\alpha}. \quad (17)$$

Once $\hat{C}_{[r_m, 2, 1]}[\alpha; 0]$ is determined, frequency estimation is given by

$$\hat{f}_b = \arg \max \left| \hat{C}_{[r_m, 2, 1]}[\alpha; 0] \right|. \quad (18)$$

TABLE II
THEORETICAL VALUE OF FOURTH-ORDER CUMULANT $|\hat{c}_{[r_m, 4, 0]}|$

$\pi/4$ -QPSK	16-PAM	QPSK	16-QAM
0.00	0.68	1.00	0.68

From (18), we obtain the second-order cycle frequency for MSK at $\hat{f}_b = 2f_s$. For QPSK, $\pi/4$ -QPSK, 16-QAM, and 16-PAM modulation formats, we get the same feature value, i.e., $\hat{f}_b = f_s$ and there is no peak for OQPSK, $\hat{f}_b = 0$ [16]. At the second-stage, to classify the remaining modulation formats, we employ the fourth-order cumulant with zero conjugations of lowpass signal $r_m[n]$. From (7), we can easily differentiate $\pi/4$ -QPSK and rest of the modulations as shown in Table II. At the final-stage, we employ eight-order cumulant given in (9) to classify QPSK, 16-PAM, and 16-QAM modulation formats.

2) *Energy Harvesting*: The received signal at EH circuit is $y_e(t) = \sqrt{\rho} y(t) + w_c(t)$. From the received signal $y_e(t)$, we can find the power for the i -th constellation point as $\mathcal{P}_{x_i}^s \approx \rho a \mathcal{P}_{x_i}$. Similar to (14), we can obtain the average harvested power $\bar{\mathcal{P}}_{\text{Eh}}^s$ as

$$\bar{\mathcal{P}}_{\text{Eh}}^s = \frac{\eta \rho}{M} \sum_{i=1}^M \left(\mathcal{P}_{x_i} \left(e^{-\frac{\mathcal{P}_1}{\rho \mathcal{P}_{x_i}}} - e^{-\frac{\mathcal{P}_2}{\rho \mathcal{P}_{x_i}}} \right) + \mathcal{P}_1 e^{-\frac{\mathcal{P}_2}{\rho \mathcal{P}_{x_i}}} \right). \quad (19)$$

C. Receiver Architecture with Energy Harvesting-based Modulation Classifier

The block diagram of SWPTMC separate receiver with EH-based modulation classifier is shown in Fig. 4. It is similar to the receiver architecture discussed in Section IV-B. Due to the PS scheme, there is always a trade-off between EH and MC performance. Therefore, we use the harvested power as additional information to improve the classification accuracy of the MC circuit. We assume the AWGN channel for this requirement because instantaneous harvested power is not constant under fading conditions, therefore can not be used as a feature extraction tool to identify the modulation formats. From the received signal $y_e(t)$, we can find the power for the

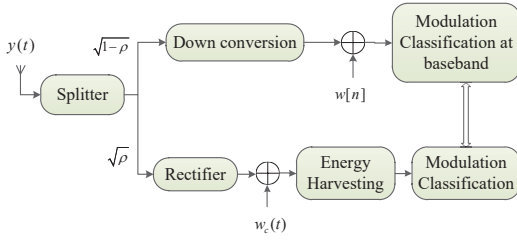


Fig. 4. Block diagram of the proposed separate receiver architecture with energy harvesting classifier.

i -th constellation point as $\mathcal{P}_{r_i}^s \approx \rho \mathcal{P}_{x_i}$. Similarly, the average harvested power $\bar{\mathcal{P}}_{\text{Eh}}^s$ over AWGN channel is obtained as

$$\bar{\mathcal{P}}_{\text{Eh}}^s = \frac{\eta\rho}{M} \sum_{i=1}^M (\mathcal{P}_{x_i} - \mathcal{P}_1 + \mathcal{P}_2). \quad (20)$$

The MC circuit uses the same classification stages as discussed in Section IV-B. It is well known that a modulation scheme with higher PAPR increases the average harvested power. To improve the classification accuracy of the MC circuit at a higher ρ , we can use the power obtained from the EH circuit as additional information. The PAPR of M-PSK, M-QAM, and M-PAM modulation formats are given by [18], $\psi_{\text{M-PSK}} = 1$, $\psi_{\text{M-QAM}} = 3\frac{\sqrt{M}-1}{\sqrt{M+1}}$, and $\psi_{\text{M-PAM}} = 3\frac{M-1}{M+1}$, respectively. Hence, the average harvested power follows: $\bar{\mathcal{P}}_{\text{Eh}}^{\text{M-PAM}} > \bar{\mathcal{P}}_{\text{Eh}}^{\text{M-QAM}} > \bar{\mathcal{P}}_{\text{Eh}}^{\text{M-PSK}}$, verified in Section V. Thus, we can use the harvested power as a feature to classify 16-PAM, 16-QAM, and PSK modulation formats.

V. SIMULATION RESULTS AND DISCUSSION

In this section, we evaluate the average harvested power and success rate of the MC for the proposed SWPTMC scheme by using Monte Carlo simulations. The IF carrier frequency, sampling rate, symbol rate, and oversampling factor are set to 3 MHz, 25 MHz, 5 MHz, and 5, respectively. However, the IF carrier and symbol rate can be varied between 1-5 MHz and sampling rate from 10-50 MHz. The roll-off factor of the RRC pulse shape filter is 0.3 and the variance of AWGN noise is calculated at 14 dB SNR. The Rayleigh fading channel with $L = 4$ channel taps is considered and the conversion efficiency, receiver RF-EH circuit thresholds \mathcal{P}_1 , and \mathcal{P}_2 are set to 0.8, 0 dBm, and 10 dBm respectively [6]. The performance is evaluated for 1000 iterations and in each iteration the number of symbols is set to 2000.

Figs. 5 and 6 show the average harvested power ($\bar{\mathcal{P}}_{\text{Eh}}$) as a function of ρ over a Rayleigh fading channel and AWGN channel, respectively. It is known that a modulation scheme with higher PAPR, increases the average harvested power as discussed in Section IV-C. Hence, the average harvested power follows: $\bar{\mathcal{P}}_{\text{Eh}}^{\text{16-PAM}} > \bar{\mathcal{P}}_{\text{Eh}}^{\text{16-QAM}} > \bar{\mathcal{P}}_{\text{Eh}}^{\text{PSKs}}$, as shown in Fig. 5 and 6.

Figs. 7 and 8 show the percentage of correct classification (P_{cc}) for the modulation formats considered, as a function of ρ over Rayleigh fading channel and AWGN channel, respectively. Receiver architectures discussed in Section IV-B

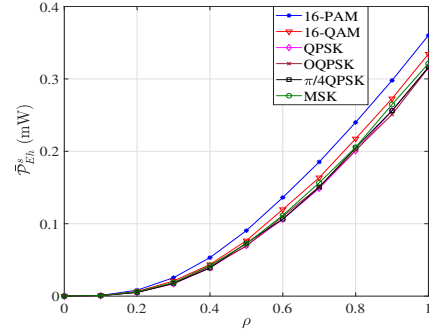


Fig. 5. Average harvested power $\bar{\mathcal{P}}_{\text{Eh}}$ versus ρ over fading channel.

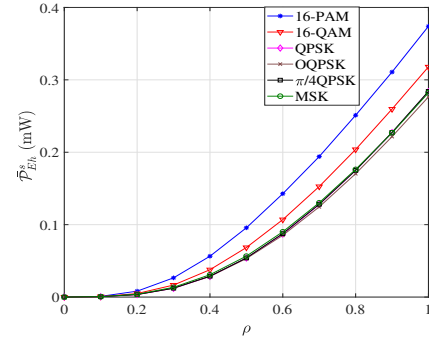


Fig. 6. Average harvested power $\bar{\mathcal{P}}_{\text{Eh}}$ versus ρ over AWGN channel.

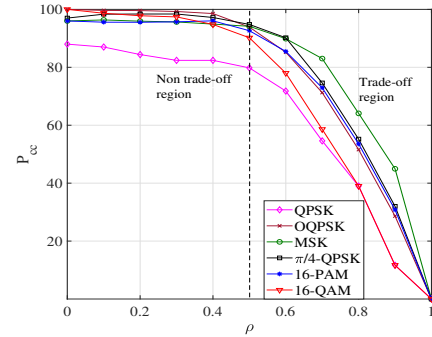


Fig. 7. Percentage of correct classification (P_{cc}) versus ρ over fading channel.

and IV-C use baseband signal to classify the modulation formats. Hence, we use PS scheme to split the received signal into two streams, one stream for the blind MC and the other stream is for EH. The classification performance trade-off has been observed for $0.5 < \rho \leq 1$. Thus, for $\rho \in [0, 0.5]$ we can simultaneously harvest power with slightly affecting the classifier performance. It has been stated earlier that the variation in the average harvested power is more noticeable over AWGN channel as shown in Fig. 6. Hence, we can use the harvested power as a feature to classify 16-PAM, 16-QAM, and QPSK variants as shown in Fig. 9.

Fig. 10 shows the P_{cc} versus SNR for the modulation formats considered. The blind MC is performed at the IF level

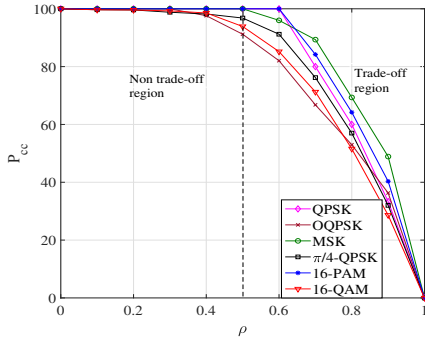


Fig. 8. P_{cc} versus ρ over AWGN channel.

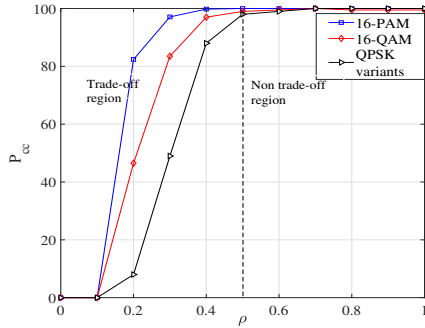


Fig. 9. EH-based classifier over AWGN: P_{cc} versus ρ .

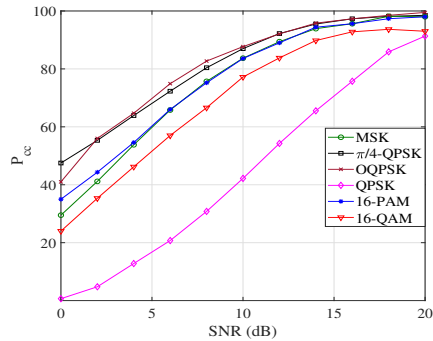


Fig. 10. P_{cc} versus SNR at the intermediate frequency level.

over Rayleigh fading channels, hence we can simultaneously perform EH and MC without the need of PS circuit as discussed in Section IV-A. It has been noted that up to 10 dB of SNR the performance increases exponentially and after then almost stable for all modulation formats except QPSK modulation format.

VI. CONCLUSION

A SWPTMC receiver architecture has been proposed and implemented for six-class of modulations over AWGN and Rayleigh fading channels. Three different receiver architectures are proposed, i.e., an integrated receiver, a separate receiver with PS, and a separate receiver with EH-based classification. The EH circuit uses a non-linear model with

a certain sensitivity and saturation level for energy harvesting and the MC circuit uses cumulants and cyclic cumulants at IF and baseband level to classify QPSK, $\pi/4$ -QPSK, OQPSK, 16-PAM, 16-QAM, and MSK modulation formats. The results highlight that for $0 < \rho \leq 0.5$ we can harvest power with slightly affecting the classifier performance. Moreover, we can improve the classification accuracy further with the EH-based classifier. Furthermore, when we employ an integrated receiver, we can simultaneously perform blind MC and harvest power without the requirement of PS circuit.

REFERENCES

- [1] B. Clerckx, R. Zhang, R. Schober, D. W. K. Ng, D. I. Kim, and H. V. Poor, "Fundamentals of wireless information and power transfer: From RF energy harvester models to signal and system designs," *IEEE J. Sel. Areas Commun.*, vol. 37, no. 1, pp. 4–33, Jan. 2019.
- [2] X. Lu, P. Wang, D. Niyato, D. I. Kim, and Z. Han, "Wireless networks with RF energy harvesting: A contemporary survey," *IEEE Commun. Surveys Tuts.*, vol. 17, no. 2, pp. 757–789, 2nd Quart. 2015.
- [3] L. R. Varshney, "Transporting information and energy simultaneously," in *Proc. IEEE Int. Symp. Inf. Theory*, Jul. 2008, pp. 1612–1616.
- [4] I. Krikidis, S. Timotheou, S. Nikolaou, G. Zheng, D. W. K. Ng, and R. Schober, "Simultaneous wireless information and power transfer in modern communication systems," *IEEE Commun. Mag.*, vol. 52, no. 11, pp. 104–110, Nov. 2014.
- [5] Z. Ding, C. Zhong, D. Wing Kwan Ng, M. Peng, H. A. Suraweera, R. Schober, and H. V. Poor, "Application of smart antenna technologies in simultaneous wireless information and power transfer," *IEEE Commun. Mag.*, vol. 53, no. 4, pp. 86–93, Apr. 2015.
- [6] Y. Dong, M. J. Hossain, and J. Cheng, "Performance of wireless powered amplify and forward relaying over nakagami- m fading channels with nonlinear energy harvester," *IEEE Commun. Lett.*, vol. 20, no. 4, pp. 672–675, Feb. 2016.
- [7] W. Liu, X. Zhou, S. Durrani, and P. Popovski, "SWIPT with practical modulation and RF energy harvesting sensitivity," in *Proc. IEEE Int. Conf. Commun.*, May 2016, pp. 1–7.
- [8] T. D. Ponnimbaduge Perera, D. N. K. Jayakody, S. K. Sharma, S. Chatzinotas, and J. Li, "Simultaneous wireless information and power transfer (SWIPT): Recent advances and future challenges," *IEEE Commun. Surveys Tuts.*, vol. 20, no. 1, pp. 264–302, 1st Quart. 2018.
- [9] L. Liu, R. Zhang, and K. Chua, "Wireless information and power transfer: A dynamic power splitting approach," *IEEE Trans. Commun.*, vol. 61, no. 9, pp. 3990–4001, Sep. 2013.
- [10] O. A. Dobre, A. Abdi, Y. Bar-Ness, and W. Su, "Survey of automatic modulation classification techniques: Classical approaches and new trends," *IET Commun.*, vol. 1, no. 2, pp. 137–156, Apr. 2007.
- [11] A. Swami and B. M. Sadler, "Hierarchical digital modulation classification using cumulants," *IEEE Trans. Commun.*, vol. 48, no. 3, pp. 416–429, Mar. 2000.
- [12] R. Gupta, S. Kumar, and S. Majhi, "Blind modulation classification for asynchronous OFDM systems over unknown signal parameters and channel statistics," *IEEE Trans. Veh. Technol.*, vol. 69, no. 5, pp. 5281–5292, Mar. 2020.
- [13] X. Yuan, Y. Li, M. Gao, T. Li, and H. Zhang, "Automatic modulation classification for MIMO-OFDM systems with imperfect timing synchronization," in *Proc. IEEE Veh. Technol. Conf.*, Sep. 2017, pp. 1–5.
- [14] S. Majhi, R. Gupta, W. Xiang, and S. Glisic, "Hierarchical hypothesis and feature-based blind modulation classification for linearly modulated signals," *IEEE Trans. Veh. Technol.*, vol. 66, no. 12, pp. 11 057–11 069, Dec. 2017.
- [15] O. A. Dobre, M. Oner, S. Rajan, and R. Inkol, "Cyclostationarity-based robust algorithms for QAM signal identification," *IEEE Commun. Lett.*, vol. 16, no. 1, pp. 12–15, Jan. 2012.
- [16] R. Gupta, S. Majhi, and O. A. Dobre, "Design and implementation of a tree-based blind modulation classification algorithm for multiple-antenna systems," *IEEE Trans. Instrum. Meas.*, vol. 68, no. 8, pp. 3020–3031, Aug. 2019.
- [17] D. R. Brillinger, *Time Series: Data Analysis and Theory*. Philadelphia, PA, USA: Soc. Ind. Appl. Math., 2001.
- [18] M. K. Simon and M. S. Alouini, *Digital Communication over Fading Channels: A Unified Approach to Performance Analysis*. Wiley, 2000.